Prediction of Pigment Epithelial Detachment in Optical Coherence Tomography Images using Machine Learning

T. M. Sheeba, S. Albert Antony Raj
Department of Computer Applications, Faculty of Science and Humanities
SRM Institute of Science and Technology, Kattankulathur - 603203, Tamil Nadu, India

***Abstract*—Pigment Epithelial Detachment (PED) is an eye condition that can affect adults over 50 and eventually harm their central vision. The PED region is positioned between the Bruch's membrane (BM) and the RPE (Retinal Pigment Epithelium) layer. Due to PED, the RPE layer is elevated arc shaped. In this paper, a method to extract the best features to detect pigment epithelial detachment (PED) is proposed. This method uses four-stage strategy that drew inspiration from OCT (Optical Coherence Tomography) imaging to detect the PED. In the first stage, to reduce the speckle-noise, in the second stage, segment the Retinal Pigment Epithelium (RPE) layer. In the third stage, a novel method is proposed to extract the best features to detect PED, and in the fourth stage, machine learning classifiers such as K-Nearest Neighbors (KNN), Logistic Regression (LR), Naïve ayes (NB), and Artificial Neural Networks (ANN) were used to significantly predict the PED. For experimental results, 150 retinal OCT volumes were used, 75 normal OCT volumes, and 75 pigment epithelial detachment volumes. Among the 150 images, 80% were used for training and 20% were used for testing. Here, there are 30 images for testing and 120 images for training. To generate a confusion matrix based on the matrices are true positive (TP), false positive (FP), true negative (TN), and false negative (FN). Logistic Regression is predicted more accuracy among the ANN, LR, NB, and KNN models. The LR model predicted accuracy 96.67% for PED detection.**

Keywords*—Artificial neural network; k-nearest neighbor; logistic regression; layer segmentation; naïve base; optical coherence tomography; pigment epithelial detachment

I. Introduction

One of the most vital and sophisticated sense organs that humans possess is the eye. In addition to aiding in object visualisation, it also improves our ability to perceive colour, light, and depth. Fig. 1 depicts a human-eye. The sclera, cornea, pupil, lens, retina, macula, optic nerve, and so on are the components of the eyes. The outer layer of the eyeball is called the sclera. Cornea is curved layer in front of the iris and pupil. The dark dot in the centre of the eye is the pupil. The coloured part of the eye is called the iris. Behind the iris lies the lens. The retina is located on the back of the eye. The retina's macula is a tiny region. The optic nerve is located in the ocular back.

In OCT images retinal layers as shown in Fig. 2. The NLF-Nerve Fibre Layer , the GCL-Ganglion Cell Layer, the IPL-Inner Plexiform Layer, the INL-Inner Nuclear Layer, the ONL-Outer Nuclear Layer, the ISPR-Inner Segment Photoreceptor Layer, the OSPR-Outer Segment Photoreceptor Layer, and the RPE-Retinal Pigment Epithelium layer.

A number of ocular illnesses, including diabetic macular edema-(DME), glaucoma and age-related macular degeneration (AMD), have been evaluated clinically using OCT. Most of the functional layers of the retina can be seen with the lately developed SD-OCT, which gives highest resolution 3D scans of the macula. For the automated segmented of the retinal layer in SD-OCT scans of healthy eyes, numerous approaches have been put forth with positive outcomes [1-15]. PEDs can be categorized as drusenoid, serous, or fibro-vascular. According to research, people with AMD and serous PED frequently already have Choroid-Neo-Vascularization (CNV) or are at a complex danger of developed it [16, 17].CNV can potentially result in significant visual acuity loss. The normal OCT images of retina is shown in Fig. 3. The abnormal (PED) image is shown in Fig. 5. The red arrow is indicated elevated RPE layer. Due to PED, the RPE layer is elevated arc shaped.

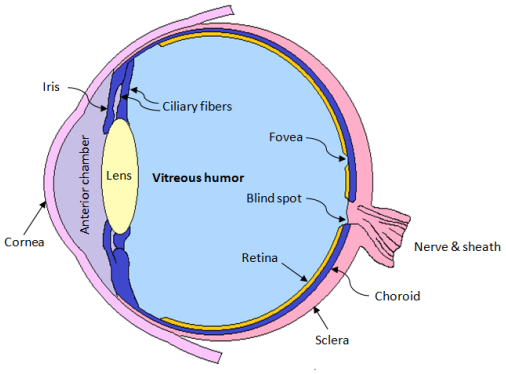

Fig. 1. Human-eye.

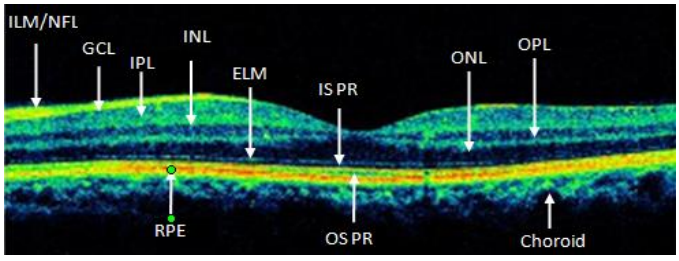

Fig. 2. OCT layers.

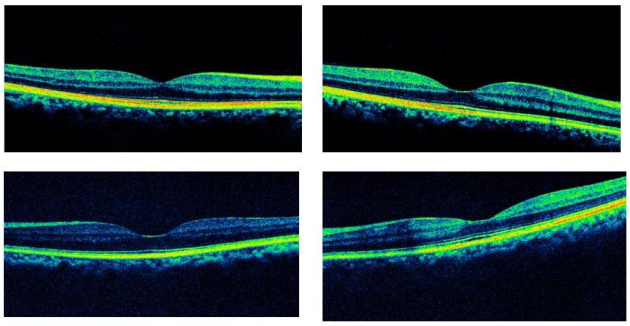

Fig. 3. OCT images of normal eye.

The separation of the retinal pigment epithelium from Bruch's membrane's inner collagenous layer is known as retinal pigment epithelial detachment. In recent years many people affected the PED. It is early diagnose easily cure the disease. This paper aims to detect the PED, Normal and PED images were classified with machine learning algorithms. This automatic model is used to assists doctors early diagnose the PED. The sample PED images are as shown in Fig. 4.

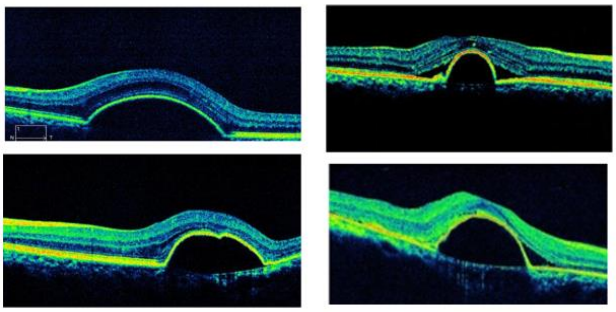

Fig. 4. PED images.

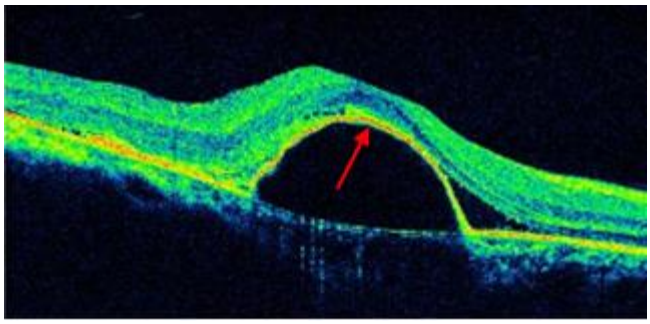

Fig. 5. OCT scan showing PED.

A wiener filter is used during pre-processing to get clear the speckles. For segment process, the threshold method is used to extract retinal layers related with RPE surface distortion. For feature extraction, the features such as Left Height (LHe), Right Height (RHe), Left Down Points (LDp) and Right Down Points (RDp) were extracted. For classification, ANN, KNN, LR and NB classifiers were used to classify the normal and PED images. Finally detected the PED, then the accuracy, sensitivity, precision and specificity were calculated based on the confusion matrix such as the FP, FN, TP and TN values. The following steps are involved to detect the PED as follows: The proposed system OCT images as input, convert OCT image into grayscale image, denoising the image, extract the RPE layer, extract the features and detect the PED.

The main contributions of this work are as follows: i) Accurately reduce the speckle noise in OCT images through the Wiener filtering technique. ii) Accurately segment the RPE layer in normal OCT images and PED images. iii) Extract four novel features to accurately predict PED disease and normal images.

II. Literature Review

Layer segmentation techniques created for retinas have also been effectively used on retinas with specific disorders such as glaucoma [11, 12, 16] and multiple abnormalies [13], or further disease in an early-stage, when there isn't a significant change in the layer structure. Segment for retina with PEDs, which are linked to sub-RPE fluid and RPE distortion. Layer segment and anomalous region segment are successfully combined where the positions of the two act as limitations on one another [17, 18]. Along with a generic method for local retinal abnormality detection, a technique for automatic characterisation of the normal retinal appearance in SD-OCT volume is provided. To reduce motion-based artefacts, the 3-D picture collection is flattened after ten intra-retinal layers are frequently segmented. To characterize the quality and width properties across the retina, 23 features are locally retrieved from the flattened OCT data in each layer. Thirteen SD-OCT volumes showing typical retinas were used to calculate the usual ranges of layer-specific feature changes.

The local variations between the usual appearance and the relevant macula parameters are subsequently classified to identify abnormalities [19]. Based on Enface fundus imaging, a unique two-stage segmentation approach was proposed. Methods: To identify fluid-associated anomalies with diffuse boundaries, the fundus picture was first segmented using a thick map [20]. The suggested approaches don't need any extra details, like layer segmentation for training. In order to smooth the segmentation map, several image segmentation techniques employ a postprocessing phase based on conditional random fields (CRF). However, first order information can only be encoded using such approaches due to computational complexity [21].

The foundation of general categorization techniques is traditional machine learning, which employs subject expertise to create hand-crafted features. To categories SRF and PED characteristic in OCT images, the authors suggested a ResidualNetworkModel [22]. In the industrialised world, AMD is the most common-source of significant vision damage in persons 50 years of older. With the development of anti-angiogenic medicines, considerable advancements in AMD treatment have been made recently, providing patients with neovascular AMD with the first realistic prospect of significant vision recovery [24].

The histologic properties of macula cell mosaics, including photoreceptor and RPE cells, can be examined in vivo using adaptive optics (AO) imaging techniques. Ophthalmic AO imaging systems produce high-resolution images that are replete with information that is challenging and/or time-

consuming to quantify manually. As a result, reliable, automated analysis systems that can deliver repeatable quantitative data regarding the examined cellular mosaics are needed. Automated algorithms have been created to locate specific photoreceptor cells, but the majority of these techniques are inadequate for describing the RPE. On simulated and actual fluorescence AO images of the RPE, built an procedure for RPE segment and demonstrate its effectiveness here [25]. For the evaluation of retinal disorders, precise segment of fluid-associated-anomalies &PED in OCT is essential [26]. A separation of the NRD from the RPE causes by sub-retinal-fluid, known as a neurosensory retinal detachment (NRD), can cause severe visual loss. It is widely known that the detachment of the neurosensory retina changes the structure and continuity of intensity of the retinal layers [27].

III. METHODOLOGY

A. Method Overview

The suggested PED detection approach includes preprocessing, RPE layer segmentation, feature extraction, training the machine learning model and PED detection as shown in Fig. 6.

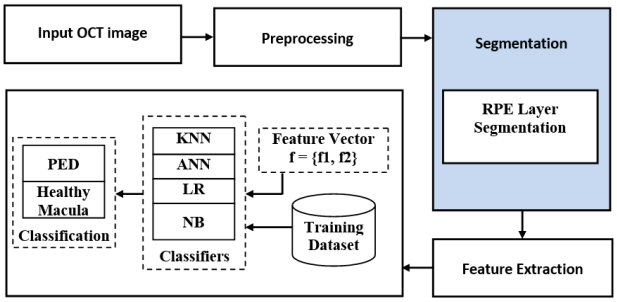

Fig. 6. Steps involved in PED detection.

In the original input OCT images the grey levels are normalised and speckle noise is reduced using wiener filter during preprocessing. An approach called the threshold method is used for RPE layer segmentation in the OCT images. PED happens at elevated RPE floors, using machine learning techniques like K-NN, LR, NB, and ANN, the characteristics retrieved and detected the PED. In order to extract features for K-NN, LR, NB, and ANN classifiers for training, OCT images are manually annotated. Then the required features are extracted which includes LH, RH, LDp and RDp which are computed from preprocessed OCT images. The machine learning models, K-NN, Logistic Regression, Nave Bayes, and ANN classifier, were trained to detect the PED. And, then trained models were used to detect PED for the new input images.

B. Pre-processing

Preprocessing is essential step to detect the PED, which is reduce the speckle-noise. The source images converted into grayscale then applying noise reduction algorithms. Speckle noise that are multiplicative in nature are more prevalent in OCT images [28-30]. The image processing and analysis techniques may perform less effectively and efficiently due to speckle, which is the primary quality degrading issue in OCT images. De-noising techniques that successfully eliminate speckle noise. Many authors suggested bilateral filtering technique and wiener filtering approach [31-36] satisfies this condition. Different filtering methods were used to eliminate the speckle-noise in the OCT images. And, analyzed mean, median, bilateral, gaussian, and wiener filtering techniques among 50 images and computed by the metrics such as PSNR, CNR and MSE. Based on the analysis, wiener filtering outperforms and significantly eliminate the speckle-noise in OCT images. Fig. 7 shows the few preprocessing images. Table I, Table II and Table III are the analysis report of wiener filtering technique. Fig. 8, Fig. 9 and Fig. 10 shows the chart of the analysis report.

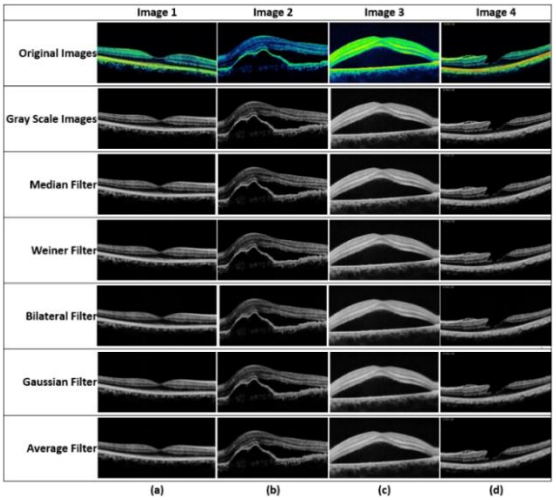

(a) Image-1, (b) Image-2, (c) Image-3, (d) Image-4

Fig. 7. Few images for pre-processing.

TABLE I. FILTERED IMAGES FOR MSE VALUE

MSE Comparison					
OCT Images	Median	**Weiner**	Bilateral	Gaussian	Average
Image 1	20.2975	**17.5117**	26.0607	27.9989	28.2926
Image 2	21.8668	**19.1076**	21.6137	30.6731	31.1288
Image 3	30.0248	**29.2978**	39.3896	45.2085	46.0353
Image 4	20.5462	**17.5784**	23.8372	29.5153	29.9617
Image 5	21.8579	**18.4743**	19.6781	29.2216	29.3958
Image 6	27.4318	**26.8242**	35.1803	40.6335	41.3365

C. RPE Layer Segmentation

RPE layer segmentation is essential step to detect the PED. Following the preprocessing step, to extract the RPE layer. Segmentation of the RPE layer is advance the procedure to separate the retinal layer [19, 20]. The threshold is one such active segmentation method, which is used to exactly separate the RPE layer. So threshold technique proposed to extract the RPE layer. As a result of the RPE layer's brightness pixel value picked up, the output is predictable and provides a clear view of the necessary retinal layers.

The thresholding method as:

$$T = T[x, y, p(x, y), f(x, y)] \quad (1)$$

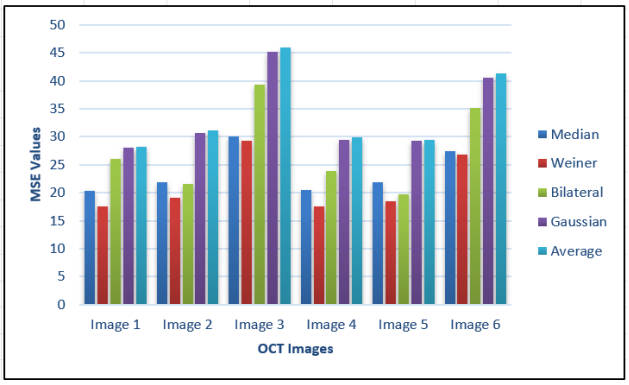

Fig. 8. Analysis chart for MSE values.

TABLE II. FILTERED IMAGES FOR PSNR VALUE

PSNR Comparison					
OCT Images	Median	**Weiner**	Bilateral	Gaussian	Average
Image 1	35.0563	**35.6975**	33.9709	33.6593	33.6140
Image 2	34.7329	**35.3187**	34.7835	33.2632	33.1991
Image 3	33.3559	**33.3166**	32.1769	31.5786	31.4998
Image 4	35.0034	**35.681**	34.3582	33.4303	33.3651
Image 5	34.7347	**35.4651**	35.1909	33.4737	33.4479
Image 6	33.7482	**33.8455**	32.6678	32.0419	31.9674

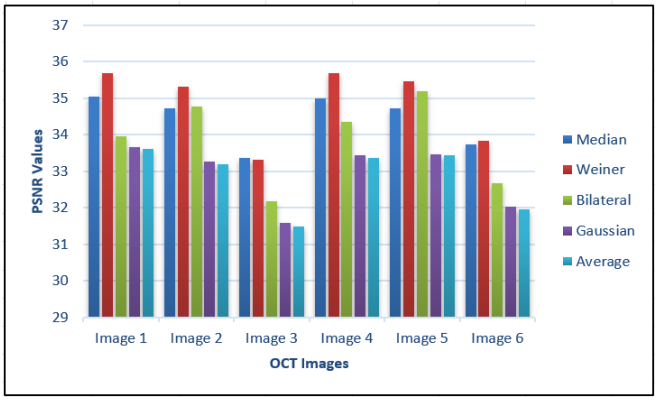

Fig. 9. Analysis chart for PSNR values.

TABLE III. FILTERED IMAGES FOR CNR VALUE

CNR Comparison					
OCT Images	Median	**Weiner**	Bilateral	Gaussian	Average
Image 1	0.01458	**-0.0008**	0.01779	0.00334	0.00345
Image 2	0.02405	**-0.0017**	0.00892	0.00436	0.00441
Image 3	0.01017	**-0.0005**	0.00303	0.00198	0.00203
Image 4	0.01696	**-0.0010**	0.00484	0.00359	0.00365
Image 5	0.01680	**-0.0003**	0.00475	0.00323	0.00332
Image 6	0.01045	**-0.0010**	0.00244	0.00217	0.00221

where, T is the threshold, and p(x, y) and f(x, y) are the greyscale images. Threshold g(x,y) is,

$$g(x,y) = \begin{cases} 1 \; if \; f(x,y) > 1 \\ 0 \; if \; f(x,y) \leq 0 \end{cases} \quad (2)$$

The Fig. 11 shows the segmented RPE layer on grayscale and original OCT images. The threshold technique compared with other methods for RPE segmentation. The Threshold technique is gave best outcome of DC and RMSE values. Table IV shows the RPE Layer Segmentation Analysis Report. Fig. 12 shows the RPE layer segmentation analysis of proposed method. Table V shows the DC and RMSE Values. Fig. 13 shows the Chart for DC and RMSE Values. Fig. 14 shows the Denoised image with histogram.

RPE layer intensity is represented by the peaks in the histogram. The background is represented by low intensity values. Choose the ideal threshold using the histogram h(i), where i= zero, 1, ..., l, and l is the highest grey level. h represent the number of pixels capturing the 'value'(i). Let the histogram L H(i) be S(t)=sum (i=t). Calculated as [42], the best threshold rate for the increasing sum of the histogram S(t) for the entire image.

$$S(T) > c, S(T+1) < c \quad (3)$$

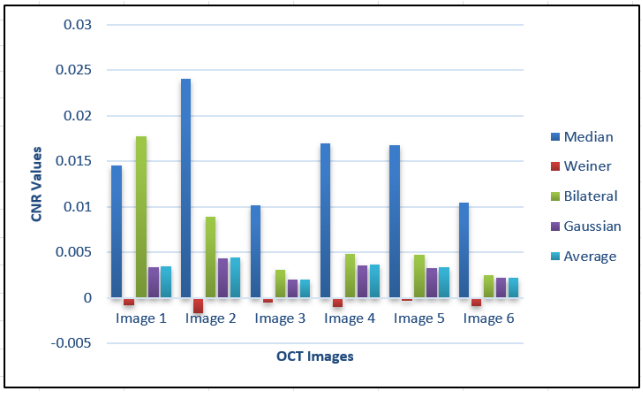

Fig. 10. Analysis chart for CNR values.

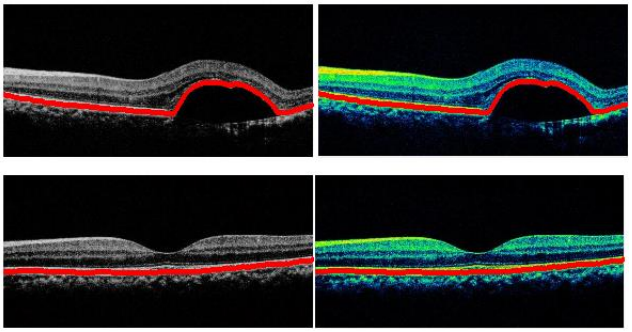

Fig. 11. RPE layer segmentation.

TABLE IV. RPE LAYER SEGMENTATION ANALYSIS REPORT

Input OCT images	**Total No. of Images**	**RPE Layer Detection**	
		No. of correct detection	**No. of incorrect detection**
Healthy Macula	20	20	0
PED Images	20	19	1

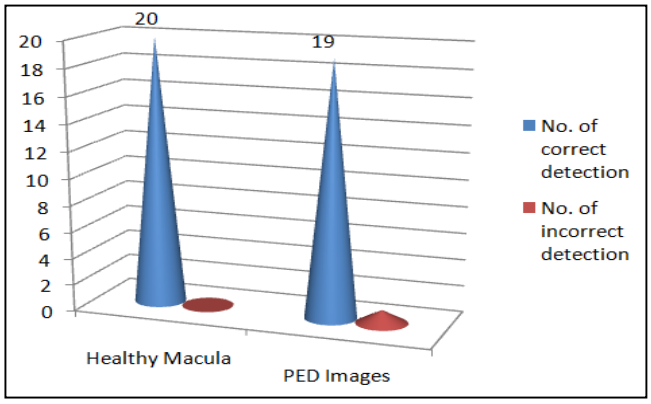

Fig. 12. RPE layer segmentation Analysis of proposed method.

TABLE V. DC AND RMSE VALUES

Method	RMSE	DC
GC[37]	0.0255	0.926
GCS[38]	0.0232	0.939
STC[39]	0.0249	0.934
LSS[40]	0.0331	0.918
RCS[41]	0.0319	0.923
Proposed Method	0.023	0.941

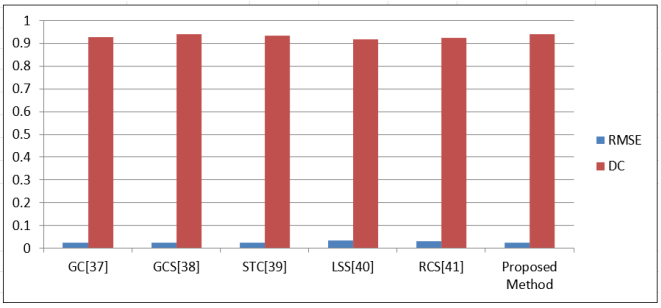

Fig. 13. Chart for DC and RMSE values.

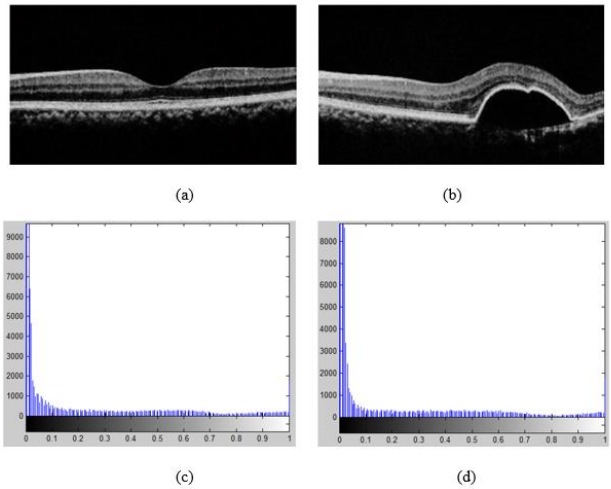

(a) Denoised healthy OCT image, (b) Denoised OCT image with PED, (c) Histogram of denoised healthy image, (d) Histogram of denoised PED image

Fig. 14. Denoised image with histogram.

where the constant,

$$c = w(\frac{t_r}{\frac{d}{r}}) + k \quad (4)$$

Here, the letters h, d, and w stand for the image's height, depth, and width, respectively. The RPE layer's thickness is measured by tr, and each image's RPE layer's slant is specified by k.

D. Feature Extraction

Feature extraction is an essential step to train and test the input using machine learning algorithms. In order to improve the performance of the machine learning algorithms to detect PED, a novel method proposed to extract best features from the segmented images. These features include LH, RH, LDp and RDp and shown in Fig. 15. These extracted features are used in the machine learning classifiers KNN, Logistic Regression, Naïve Base and ANN to detect PED. The outcome of the classifier algorithms are corresponded the features of data is obtainable to them in order to fix the TN, FP, TP and FN [21-23]. Accuracy, sensitivity and specificity are evaluated for the classifier independently using these metrics, and the results are then used to categorise the performance of the classifier.

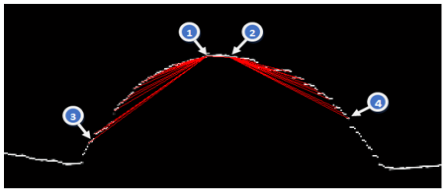

1→ Left Height 2 → Right height
3 → Left Down Points 4 → Right Down Points

Fig. 15. Extracted features.

Here, the following formulae used to fix the top, bottom, and maximum height of the RPE layer:

$$t = min(L_i) \quad (5)$$

$$b = max(L_i) \quad (6)$$

$$maxHgt = b - t \quad (7)$$

where, Li is the axis-y values for each-x-values on the RPE- layer and x ranges from 0 to the image width. Since the image's top left coordinate is (0, 0), the min-function is used to obtain the RPE-layer's smallest axis-y values in-order-to establish the layer's top. The lowest layer is found using the max function. Repeating the line-no from zero to the top left-point brings it to its highest position. Moving periodically as of the projected top-left-point to the line's largest point yields the top right-point. Next, a bounding rectangle is created by extracting 20 points from the upper left-point. The height of the retinal layer determines the rectangle's width.

$$w = mH \quad (8)$$

Twenty-point were deducted from the top-left-points and twenty-point from the top-right points in order to determine the curve in this investigation. The distance is computed in the following way to extract 20 points from the top-left-points:

$$d = \frac{w}{20} \quad (9)$$

The line-heights of each-points is then calculated by iterating the line points 20 times backward from the top left point:

$$lPs_i = mHgt - (L_{(topLPoint-d*i)}) \quad (10)$$

where, i differs from one to 20.

The below calculation extracts the top-right 20 points:

$$rPs_i = mHgt - (L_{(topRPoint+d*i)}) \quad (11)$$

This ranges from 1 to 20 for i.

The following formulas are used to extract the features of left height (LHe) and right height (RHe):

$$LHe = max(lPoints_i) \quad (12)$$

$$RHe = max(rPoints_i) \quad (13)$$

Next, the consecutive leftPoints are compared in order to derive the left down points (LDp) characteristic. Increase the counter LDp if a leftpoint-values is smaller than the leftpoint-values that comes after it. By comparing the rightPoint and rising the counter, the right-down-point (RDp) representative is determined.

$$LDP = LDP + 1 \quad if(lPoints_i < lPoints_{(i+1)}) \quad (14)$$

$$RDP = RDP + 1 \quad if(RPoints_i < RPoints_{(i+1)}) \quad (15)$$

Algorithm Feature_Extraction(Lineseg)

INPUT:
LineSeg – Extracted RPE layer in an array
OUTPUT:
LHe – Left height
RHe – Right height
LDp – Left down points
RDp – Right down points

1. t = minimum(LineSeg)
2. b = maximum(LineSeg)
3. lineHgti = b - LineSegi;
4. maxHgt = b - t;
5. Repeat line-6 for j=1 to sizeof(LineSeg)
6. if (lineHgti == maxHgt) goto line-7
7. topLPoint = j
8. w = maxHgt
9. Pts=20
10. d = w / Pts;
11. leftPts(1)=maxHgt;
12. Repeat 13 to 14 for p =1 to Pts
13. pos1 = tpLPoint - disBtwnPts*j;
14. leftPts(j+1)=lineHgt(pos1);
15. Repeat 16 for p = j to sizeof(lineHgt)
16. if (lineHgt(k) <> maxHgt) goto 17
17. tpRPoint = p;
18. rightPts(1)=maxHgt;
19. Repeat 20 to 21 for q=1 to Pts
20. pos1=tpRPoint + disBtwnPts * q
21. rightPts(q+1) = lineHgt(pos1)
22. LHe = maxi(leftHgt)
23. RHe = maxi(rightHgt)
24. LDp = 0
25. RDp = 0
26. Repeat 27 to 30 for k = 2 to Pts
27. if ((leftHgtk-leftHgtk-1) > 0)
28. LDp++
29. if ((rightHgtk – rightHgtk-1) > 0)
30. RDp++
31. Stop

E. Classification

In this paper, to detect the PED from the RPE layer 4 features, such as LH, RH, LDp and RDp were extracted. The extracted four features were used to classify normal and abnormal OCT images. To assess the discriminative power of projected feature signifiers, both parametric and non-parametric classifiers are examine to PED, such as KNN, LR, Naïve Baye and ANN. Here these four classification procedures, such as KNN, LR, NB and ANN, were compared. The LR classifier gave best outcome when compared with the other three classifiers. To calculate accuracy, sensitivity, specificity, precision, Recall and F1-score, the following formulas were used:

$$Accuracy = \frac{TruePositive + TrueNegative}{TruePositive + TrueNegative + FalsePositive + FalseNegative}$$

$$Sensitivity = \frac{TruePositive}{TruePositive+FalseNegative} \quad (16)$$

$$Specificity = \frac{TrueNegative}{TrueNegative+FalsePositive} \quad (17)$$

$$Precision = \frac{TruePositive}{TruePositive+FalsePositive} \quad (18)$$

$$Recall = \frac{TruePositive}{TruePositive+FalseNegative} \quad (19)$$

$$F1\_score = \frac{2*Precision*Recall}{Precision+Recall} \quad (20)$$

IV. Result and Discussion

In this work, 150 OCT images used, 75 normal and 75 abnormal OCT images. In the proposed methodology 80 percentage of the images were used for training, while 20 percentage were used for testing and validations. Out of the entire 150 OCT images, 120 used for training and 30 for testing. In order to remove speckle-noise and segment the image, the image was first converted to grayscale and preprocessed using a wiener filtering. After denoising extract the RPE-layer. Segmented the RPE-layer used to the threshold technique. Four features such as LH, RH, LDp and RDp were extracted from the segmented OCT images, and these features showed to have a notable difference between the normal and PED images. The KNN, Naive Bayes, Logistic Regression and ANN classifiers were fed the collected features, and the results are represented as TP, TN, FP, and FN as in Table VI. TP, FN, TN and FP are the evaluation metrics of the classifiers as shown in Fig. 16.

TABLE VI. RESULTS OF K-NN, LR, NB AND ANN

Classification Metrics	K-NN	Logistic Regression	Naïve Base	ANN
TP	13	15	15	15
FN	2	0	0	0
TN	13	13	15	13
FP	2	2	0	2

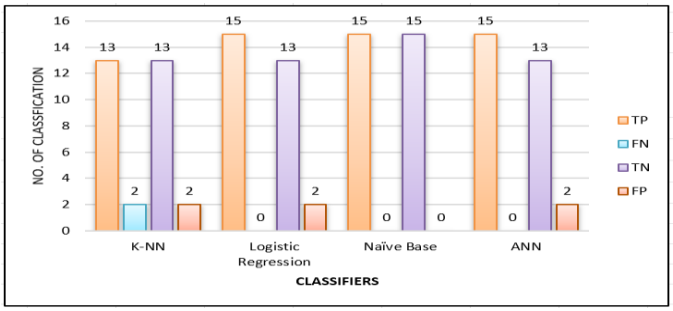

Fig. 16. Evaluation results of K-NN, LR, NB and ANN.

The findings of the overall system performance research in terms of sensitivity, specificity, accuracy, precision, and F1 score are presented in Table VII. The analysis report of NB, KNN, LR and ANN is shown in Fig. 17. It is clear from the overall findings that the Logistic Regression Classifier appears to produce more accurate results than the KNN, ANN, and Naive Base Classifications. The entire system parameters like sensitivity, specificity, precision, F1 score and accuracy.

TABLE VII. CLASSIFICATION METRICS OF NB, LR, KNN AND ANN

Classification Metrics	NB	KNN	LR	ANN
Accuracy	93.00	86.67	96.67	93.33
Sensitivity	100.00	86.67	100.00	100.00
Specificity	86.67	86.67	93.33	86.67
Precision	88.24	86.67	93.75	88.24
F1 score	93.75	86.67	96.77	93.75

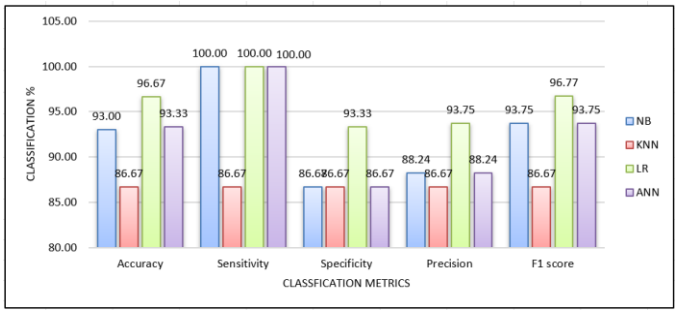

Fig. 17. Classification metrics of NB, KNN, LR and ANN.

Based on the Table VII, KNN produces the result for 86.67% Accuracy, 86.67% Sensitivity, 86.67% Specificity, Precision 86.67% and F1 score 86.67%, Naïve Base produces the result for Accuracy 93%, Sensitivity 100%, Specificity 86.67%, Precision 88.24% and F1 score 93.75%, ANN produces the result Accuracy 93.33%, Sensitivity 100%, Specificity 86.67%, Precision 88.24% and F1 score 93.75% and Logistic Regression produces the result Accuracy 96.67%, 100%Sensitivity, 93.33% Specificity, 93.75% Precision and 96.77% F1 score . The confusion matrix of these classifiers are shown in Fig. 18, Fig. 19, Fig. 20 and Fig. 21 and also analyses the metric ROC curve from the confusion matrix are shown in Fig. 22, Fig. 23 and Fig. 24. Area under curve (AUC) for LR is 0.9939393939393939, KNN is 0.9484848484848486 and NB is 0.9939393939393939.

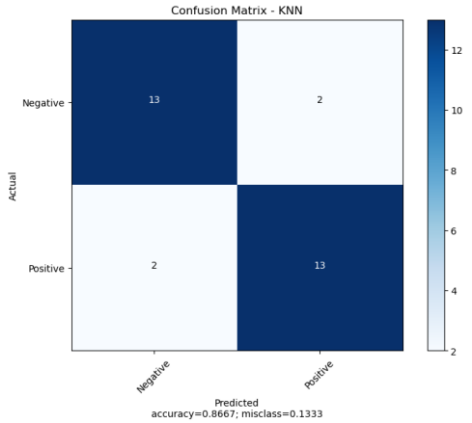

Fig. 18. Confusion matrix for KNN.

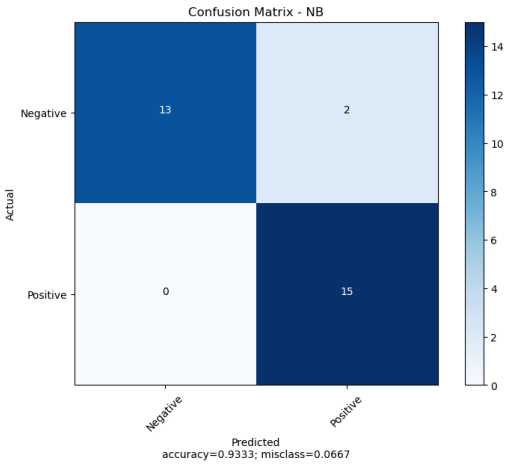

Fig. 19. Confusion matrix for NB.

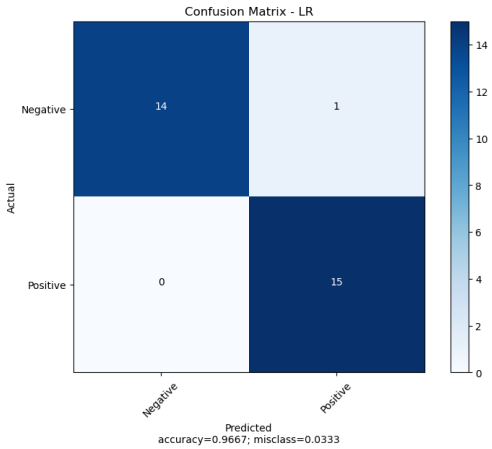

Fig. 20. Confusion matrix for LR.

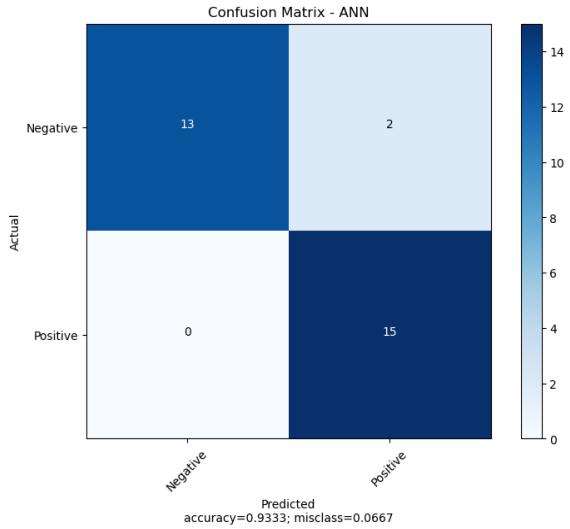

Fig. 21. Confusion matrix for ANN.

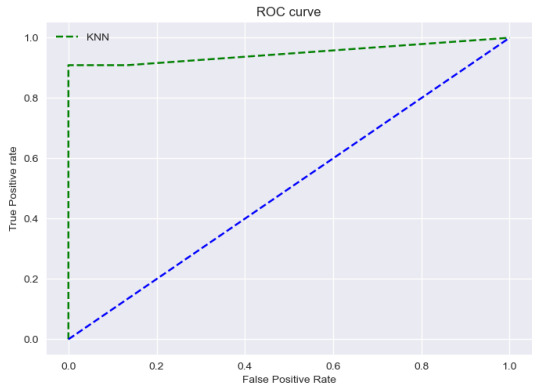

Fig. 22. ROC for KNN, AUC for 0.9484848484848486.

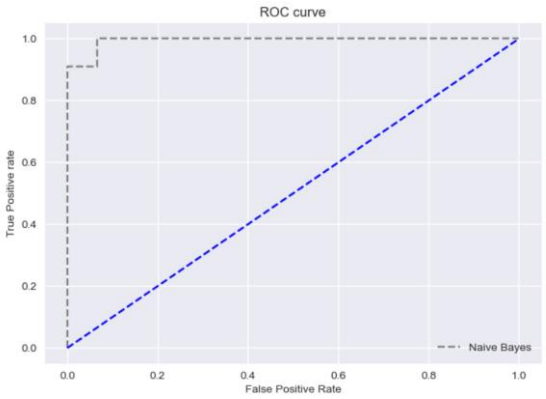

Fig. 23. ROC for NB, AUC for 0.9939393939393939.

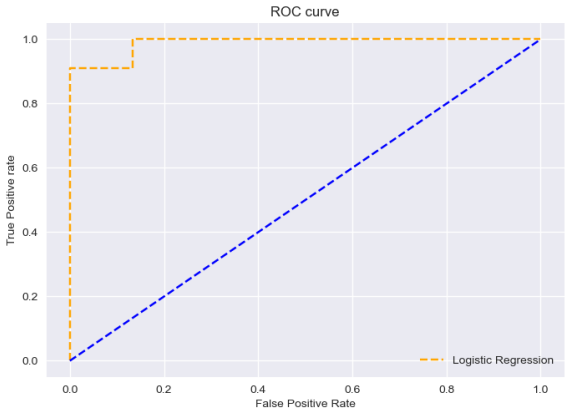

Fig. 24. ROC for LR, AUC for 0.9939393939393939.

V. CONCLUSION

The main contributions of this work are: accurately reduce the speckle noise in OCT images, accurately segment the RPE layer in normal OCT images and PED images, and extract four novel features to accurately predict PED disease and normal images. Through the experimental results, Wiener filtering technique outperforms in reduce speckle noise in the OCT images. The suggested technique and steps appear to be effective for extracting best features from the RPE layer for detecting PED in OCT images. These features were used to train the classifiers and tested with new inputs. Based on these features, the performance of logistic regression classifier was better when compared with other classifiers. The degree of precision attained demonstrates that the technique can also be used in practical applications. To accurately and completely examine the actual performance, the usefulness of the suggested classifier systems must be assessed for specific abnormality-based categorization, such as PED. The normal and PED images were classified with machine learning algorithms. This automatic model is used to assists doctors early diagnose the PED. In this paper, the machine learning classifiers like KNN, LR, NB and ANN were compared. KNN produces the result for Accuracy 86.67%, Sensitivity 86.67%, Specificity 86.67%, Precision 86.67% and F1 score 86.67%, LR produces the result for Accuracy 96.67%, Sensitivity 100%, Specificity 93.33%, Precision 93.75% and F1 score 96.77%, and NB produces the result Accuracy 93.33%, Sensitivity 100%, Specificity 86.67%, Precision 88.24% and F1 score 93.75% and ANN found 93.33% accuracy, 100% sensitivity, 86.67% specificity, 88.245 precision and F1 score 93.75%. Based on the experiments, it is found that logistic regression classifier gives high accuracy in identifying PED illnesses and broadening the scope of anomalies. Further this study can be extended to detect the PED using other machine learning algorithms. Deep learning can also be used in future to detect PED in retinal OCT images.

REFERENCES

[1] M. K. Garvin, M. D. Abràmoff, R. Kardon, S. R. Russell, X. Wu, and M. Sonka, "Intraretinal layer segmentation of macular optical coherence tomography images using optimal 3-D graph search," IEEE Trans. Med. Imag., vol. 27, no. 10, pp. 1495–1505, Oct. 2008.

[2] M. K. Garvin, M. D. Abràmoff, X. Wu, S. R. Russell, T. L. Burns, and M. Sonka, "Automated 3-D intraretinal layer segmentation of macular spectral-domain optical coherence tomography images," IEEE Trans. Med. Imag., vol. 28, no. 9, pp. 1436–1447, Sep. 2009.

[3] K. Lee, "Segmentations of the intraretinal surfaces, optic disc and retinal blood vessels in 3D-OCT scans," Ph.D. dissertation, Univ. Iowa, Iowa City, 2009.

[4] S. Lu, C. Y. Cheung, J. Liu, J. H. Lim, C. K. Leung, and T. Y. Wong, "Automated layer segmentation of optical coherence tomography images," IEEE Trans. Biomed. Eng., vol. 57, no. 10, pp. 2605–2608, Oct. 2010.

[5] A. Yazdanpanah, G. Hamarneh, B. R. Smith, and M. V. Sarunic, "Segmentation of intra-retinal layers from optical coherence tomography images using an active contour approach," IEEE Trans. Med. Imag., vol. 30, no. 2, pp. 484–496, Feb. 2011.

[6] Q. Song, J. Bai, M. K. Garvin, M. Sonka, J. M. Buatti, and X. Wu, "Optimal multiple surface segmentation with shape and context priors," IEEE Trans. Med. Imag., vol. 32, no. 2, pp. 376–386, Feb. 2013.

[7] P. A. Dufour, L. Ceklic, H. Abdillahi, S. Schröder, S. De Dzanet, U. Wolf-Schnurrbusch, and J. Kowal, "Graph-based multi-surface segmentation of OCT data using trained hard and soft constraints," IEEE Trans. Med. Imag., vol. 32, no. 3, pp. 531–543, Mar. 2013.

[8] Q. Yang, C. A. Reisman, Z. Wang, Y. Fukuma, M. Hangai, N. Yoshimura, A. Tomidokoro, M. Araie, A. S. Raza, D. C. Hood, and K. Chan, "Automated layer segmentation of macular OCT images using dual-scale gradient information," Opt. Exp., vol. 18, pp. 21 293–307, 2010.

[9] S. J. Chiu, X. T. Li, P. Nicholas, C. A. Toth, J. A. Izatt, and S. Farsiu, "Automatic segmentation of seven retinal layers in SDOCT images congruent with expert manual segmentation," Opt. Exp., vol. 18, no. 18, pp. 19413–28, 2010.

[10] J. Novosel, K. A. Vermeer, G. Thepass, H. G. Lemij, and L. J. van Vliet, "Loosely coupled level sets for retinal layer segmentation in optical coherence tomography," in Proc. IEEE Int. Symp. Biomed. Imag., 2013, pp. 1010–1013.

[11] K. A. Vermeer, J. van der Schoot, H. G. Lemij, and J. F. de Boer, "Automated segmentation by pixel classification of retinal layers in ophthalmic OCT images," Biomed. Opt. Exp., vol. 2, pp. 1743–56, 2011.

[12] R. Kafieh, H. Rabbani, M. D. Abramoff, and M. Sonka, "Intra-retinal layer segmentation of 3D optical coherence tomography using coarse grained diffusion map," Med. Image Anal., vol. 17, pp. 907–928, 2013.

[13] A. Lang, A. Carass, M. Hauser, E. S. Sotirchos, P. A. Calabresi, H. S. Ying, and J. L. Prince, "Retinal layer segmentation of macular OCT images using boundary classification," Biomed. Opt. Exp., vol. 4, pp. 1133–52, 2013.

[14] The Iowa Reference Algorithms. Iowa City, IA, Iowa Inst. Biomed. Imag. [Online]. Available: http://www.biomed- imaging.uiowa.edu/ downloads/

[15] X. Chen, P. Hou, C. Jin, W. Zhu, X. Luo, F. Shi, M. Sonka, and H. Chen, "Quantitative analysis of retinal layers' optical intensities on 3D optical coherence tomography," Invest. Ophthalmol. Vis. Sci., vol. 54, no. 10, pp. 6846–6851, Oct. 2013.

[16] S. Zayit-Soudry, I. Moroz, and A. Loewenstein, "Retinal pigment epithelial detachment," Surv. Ophthalmol., vol. 52, no. 3, pp. 227–243, May-Jun. 2007.

[17] P. A. Keane, P. J. Patel, S. Liakopoulos, F. M. Heussen, S. R. Sadda, and A. Tufail, "Evaluation of age-related macular degeneration with optical coherence tomography," Surv. Ophthalmol., vol. 57, no. 5, pp. 389–414, Sep.-Oct. 2012.

[18] Fei Shi, Xinjian Chen, Heming Zhao, Weifang Zhu, Dehui Xiang, Enting Gao, Milan Sonka and Haoyu Chen, "Automated 3-D Retinal Layer Segmentation of Macular Optical Coherence Tomography Images With Serous Pigment Epithelial Detachments", IEEE Transactions On Medical Imaging, Vol. 34, No. 2, February 2015.

[19] Quellec G, Lee K, Dolejsi M, Garvin MK, Abràmoff MD, Sonka M. Three-dimensional analysis of retinal layer texture: identification of fluid-filled regions in SD-OCT of the macula. IEEE Trans Med Imaging. 2010 Jun;29(6):1321-30. doi: 10.1109/TMI.2010.2047023. Epub 2010 Apr 1. PMID: 20363675; PMCID: PMC2911793.

[20] Wu M, Chen Q, He X, Li P, Fan W, Yuan S, Park H. Automatic Subretinal Fluid Segmentation of Retinal SD-OCT Images With Neurosensory Retinal Detachment Guided by Enface Fundus Imaging. IEEE Trans Biomed Eng. 2018 Jan;65(1):87-95. doi: 10.1109/TBME.2017.2695461. Epub 2017 Apr 18. PMID: 28436839.

[21] R. Tennakoon, A. K. Gostar, R. Hoseinnezhad and A. Bab-Hadiashar, "Retinal fluid segmentation in OCT images using adversarial loss based convolutional neural networks," 2018 IEEE 15th International Symposium on Biomedical Imaging (ISBI 2018), 2018, pp. 1436-1440, doi: 10.1109/ISBI.2018.8363842.

[22] Y. Huang and J. Hu, "Residual Neural Network Based Classification of Macular Edema in OCT," 2019 IEEE 31st International Conference on Tools with Artificial Intelligence (ICTAI), 2019, pp. 736-743, doi: 10.1109/ICTAI.2019.00107.

[23] T. M. Sheeba & S. Alber Antony Raj "Distinct Features for Detection of Pigment Epithelial Detachment using Machine Learning and Artificial Neural Network in Two-Dimensional Optical Coherence Tomography Images". International Journal of Intelligent Systems and Applications in Engineering, 12(14s), 338–347, 2024.

[24] Keane PA, Patel PJ, Liakopoulos S, Heussen FM, Sadda SR, Tufail A. Evaluation of age-related macular degeneration with optical coherence tomography. Surv Ophthalmol. 2012 Sep;57(5):389-414. doi: 10.1016/j.survophthal.2012.01.006. PMID: 22898648.

[25] Rangel-Fonseca P, Gómez-Vieyra A, Malacara-Hernández D, Wilson MC, Williams DR, Rossi EA. Automated segmentation of retinal pigment epithelium cells in fluorescence adaptive optics images. J Opt Soc Am A Opt Image Sci Vis. 2013 Dec 1;30(12):2595-604. doi: 10.1364/JOSAA.30.002595. PMID: 24323021.

[26] Chen X, Niemeijer M, Zhang L, Lee K, Abramoff MD, Sonka M. Three-dimensional segmentation of fluid-associated abnormalities in retinal OCT: probability constrained graph-search-graph-cut. IEEE Trans Med Imaging. 2012 Aug;31(8):1521-31. doi: 10.1109/TMI.2012.2191302. Epub 2012 Mar 19. PMID: 22453610; PMCID: PMC3659794.

[27] L. Bekalo et al., "Automated 3-D Retinal Layer Segmentation From SD-OCT Images With Neurosensory Retinal Detachment," in IEEE Access, vol. 7, pp. 14894-14907, 2019, doi: 10.1109/ACCESS.2019.2893954.

[28] Sun S, Guo Q, Lei B, Gao BZ, Dong F. Image denoising algorithm based on contourlet transform for optical coherence tomography heart tube image. IET Image Process. 2013; 7(5), pp. 442–450.

[29] Avanaki MRN, Cernat R, Tadrous PJ, Tatla T, PodoleanuAG, Ali Hojjatoleslami S, Spatial compounding algorithm for speckle reduction of dynamic focus OCT images. IEEE Photonics TechnolLett. 2013; 25(15), pp. 1439–1442.

[30] Manojlovic LM. Novel Method for Optical Coherence Tomography Resolution Enhancement.IEEE J. Quantum Electron. 2011; 47(3),pp. 340–347.

[31] C. Tomasi and R. Manduchi, "Bilateral filtering for gray and color images," in Proc. IEEE Int. Conf. Comput. Vis., 1998, pp. 839–846.

[32] M. Anand, C. Jayakumari, "Automated Detection of Macular Hole in Optical Coherence Tomography Images using Depth-Check Algorithm", International Journal of Engineering and Advanced Technology (IJEAT) ISSN: 2249 – 8958, Volume-9 Issue-1, October 2019.

[33] M. Anand, C. Jayakumari," A Novel Depth-Check Algorithm to Detect Macular Hole from Optical Coherence Tomography Images", International Journal of Innovative Technology and Exploring Engineering (IJITEE) ISSN: 2278-3075, Volume-8 Issue-12, October 2019.

[34] M. Anand, C. Jayakumari," Automated detection of full thickness macular hole in optical coherence tomography images", Journal of International Pharmaceutical Research, ISSN: 1674-0440.

[35] M. Anand, C. Jayakumari," A New Approach to Detect Macular Hole from Optical Coherence Tomography Images", Indian Journal of Public Health Research & Development, July 2019, Vol.10, No. 7.

[36] T.M. Sheeba and S. Albert Antony Raj ," Analysis of Noise Removal Techniques on Retinal Optical Coherence Tomography Images", (IJACSA) International Journal of Advanced Computer Science and Applications, Vol. 13, No. 9, 2022.

[37] Bashir Isa Dodo , Yongmin Li, Djibril Kaba , And Xiaohui Liu, "Retinal Layer Segmentation in Optical Coherence Tomography Images", IEEE Access, VOLUME 7, Oct-2019, pp. 152388-152398.

[38] Qifeng Yana , Bang Chena, Yan Hub , Jun Chengc , Yan Gongd , Jianlong Yanga , Jiang Liub and Yitian Zhaoa, "Speckle reduction of OCT via super resolution reconstruction and its application on retinal layer segmentation", Artificial Intelligence In Medicine, 2020, pp. 1-10.

[39] S. J. Chiu, X. T. Li, P. Nicholas, C. A. Toth, J. A. Izatt, and S. Farsiu, ''Automatic segmentation of seven retinal layers in SDOCT images congruent with expert manual segmentation,'' Opt. Express, vol. 18, no. 18, pp. 19413–19428, 2010.

[40] B. I. Dodo, Y. Li, X. Liu, and M. I. Dodo, ''Level set segmentation of retinal OCT images,'' in Proc. 12th Int. Joint Conf. Biomed. Eng. Syst. Technol., vol. 2, 2019, pp. 49–56.

[41] B. I. Dodo, Y. Li, K. Eltayef, and X. Liu, ''Graph-cut segmentation of retinal layers from OCT images,'' in Proc. 11th Int. Joint Conf. Biomed. Eng. Syst. Technol. (BIOIMAGING), vol. 2, 2018, pp. 35–42.

[42] Samra Naz, Aneeqa Ahmed, M. Usman Akram, Shoab A. Khan, "Automated Segmentation of RPE Layer for the Detection of Age Macular Degeneration Using OCT Images", 978-1-4673-8910-5/16/$31.00 ©2016 IEEE.